MASTER OSCILLATOR TECHNIQUES FOR 10 MICRON RADAR

A. Stein

United Aircraft Research Laboratories

Prepared for:

Office of Naval Research
Advanced Research Projects Agency

31 March 1973

M921512-3

MASTER OSCILLATOR TECHNIQUES FOR 10 micron RADAR

Semi-Annual Technical Report

Period Covered 25 August 1972 to 25 March 1973

CONTRACT NO. N00014-73-C-0086

PREPARED FOR

Advanced Research Projects Agency

ARPA ORDER NO. 1806, AMENDMENT NO. 6

United Aircraft
Research Laboratories

UNITED AIRCRAFT CORPORATION

EAST HARTFORD, CONNECTICUT 06108

Details of illustrations in this document may be better studied on microfiche

M921512-3

Interim Technical Report

Master Oscillator Techniques For 10 Micron Radar

by

A. Stein
United Aircraft Research Laboratories
East Hartford, Connecticut 06108
(203) 565-4428

March 31, 1973

Prepared for the Office of Naval Research
Scientific Contracting Officer-Dr. M. White
Contract N00014-73-C-0086 - $94,247.00
25 August 1972 to 23 August 1973

Sponsored by
Advanced Research Projects Agency
ARPA Order 1806, Amendment No. 6, 7-18-72

TABLE OF CONTENTS

LIST OF ILLUSTRATIONS

1.0 SUMMARY

A CO_2 waveguide laser was operated with an intracavity electro-optic polarization modulator. Coupling modulation at 48 and 120 MHz was observed which represents a significant step towards the contract goal to investigate the feasibility of linear ramp frequency modulation (500 MHz in 300 μsec) of a stable CO_2 oscillator. This master oscillator is of interest for a high resolution optical radar application.

Coupling modulation offers the possibility of obtaining an efficient carrier suppressed AM modulation. By sweeping the modulation frequency the AM sidebands are swept accordingly. Considering, then, one sideband only, it is apparent that it represents a frequency chirped signal. To separate one sideband from the other the carrier position is shifted to the wings of the laser gain profile, such that one of the AM sidebands coupled from the master oscillator is inside while the other is outside the active gain profile of the P(20) line. If the output of the master oscillator is fed into a CO_2 laser amplifier chain, as in the envisaged radar transmitter, only one sideband is amplified.

During the next reporting period the present CO_2 waveguide laser will be modified to provide line and mode selection for the required carrier frequency control.

2.0 BACKGROUND

2.1 General

A stable master oscillator is required for application in a high resolution optical radar which employs the so-called "delay doppler mapping" technique and involves accurate simultaneous measurements of both doppler and range. The desired imaging waveform consists of a series of 128 equally spaced pulses (Fig. 2-1). The overall waveform as well as the individual pulse profile are truncated gaussians. During each pulse the optical frequency is swept linearly through a 500 MHz range centered about the P(20) CO_2 laser line, and the frequency chirp is timed such that the center frequency of the chirp appears at the peak of each pulse. The length of the overall imaging signal is variable between 64 μsec and 4.8 msec and the repetition frequency of the imaging waveform is 10 Hz.

To obtain the required range accuracy of 0.5 m the rms deviation of each frequency ramp from linear and the cumulative error must be less than 6 MHz. Timing of the ramp initiation must be accurate to better than 3 nsec.

Carrier amplitude and phase stability affect the cross range resolution. For a perfectly stable carrier, the cross range resolution is limited by the waveform envelope only, i.e., by the corresponding spectral characteristic. To ensure that the actual spectral distribution does not deviate by more than 2 dB from the envelope limited case, down to - 40 dB from the peak, a carrier stability of 200 Hz is required for the duration of the imaging signal, i.e., 5 msec or less.

By using coupling modulation and a frequency swept rf drive signal, it is possible, in principle, to lock the laser to an ultrastable optical local oscillator and provide a stable carrier such that the optical sidebands precisely reflect the modulation signal. The use of an intracavity modulator offers a considerable increase in modulation efficiency and output power over external mixing, but care must be taken to avoid carrier instability due to electro-optic and thermo-optic effects in the modulator crystal. Because of the linear relationship between output and modulation power, this technique also permits a straightforward generation of the required waveform and pulse envelope by selecting the modulation intensity waveform accordingly.

At present, UARL has assembled and tested a high-pressure CO_2 waveguide laser and is observing coupling modulation with the help of an intracavity CdTe electro-optic modulator. Figure 2.2 shows a photograph and schematic drawing of the system. It consists of a waveguide CO_2 plasma tube, two resonator mirrors and an intracavity CdTe modulator.

FIG. 2-1

RADAR IMAGING SIGNAL

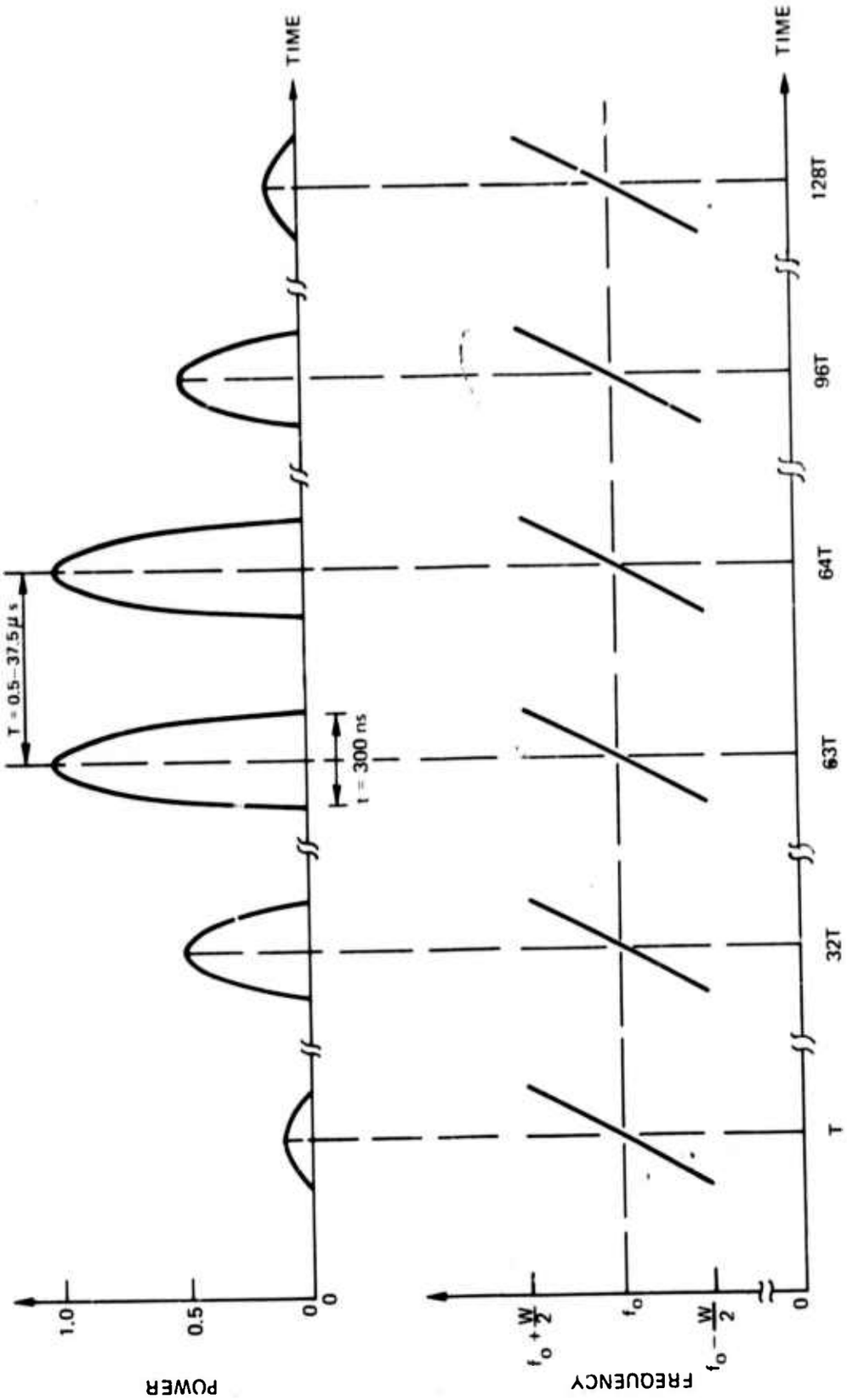

Coupling modulation involves partial depolarization of a laser mode proportional to the square of the rf voltage applied to the electro-optic crystal (Ref. 1). The light beam then contains components of parallel and orthogonal polarization relative to the orientation of an intracavity Brewster plate. Coupling of the orthogonally polarized radiation from the resonator occurs by Fresnel reflection off this plate. For the here considered electro-optic effect and in the absence of a dc bias, the parallel field components are amplitude modulated at twice the applied frequency, as shown in Fig. 2-2. The carrier is constant and may be locked to an outside standard such as a second laser serving as an optical local oscillator. In the absence of a bias, the orthogonal polarization component is a suppressed carrier AM modulated signal. By frequency sweeping the rf drive, the AM sidebands are frequency chirped in opposite directions.

To obtain proper spectral match to the gain band of the optical radar power amplifiers, the frequency chirp of one of these AM sidebands must be centered on the P(20) laser line. For the master oscillator considered here this is accomplished by obtaining laser oscillation at an axial resonance displaced from line center such that the selected AM sideband sweeps through the amplifier gain band in the above described fashion, while the other sideband remains outside the active spectrum (Fig. 2-3).

To implement the required carrier offset, a wide band oscillator, such as a waveguide laser whose active transition is collision broadened to a 1 GHz bandwidth at 200 torr operating pressure, is made to oscillate at an axial resonance displaced from line center.

Ideally, one would like to arrange for a large axial mode spacing to insure that only one axial resonance falls within the active spectrum, thus eliminating mode selection. Since the final application as presently conceived calls for a 1.5 GHz frequency chirp, it would require a resonator of less than 10 cm optical length which does not seem feasible considering that the optical length of the present modulator crystal alone exceeds that value. The presence of several axial resonances inside the active spectrum then requires proper axial mode selection to obtain oscillation of the desired frequency rather than at the resonance closest to line center.

Line and mode selection is accomplished by replacing the output mirror with a Fabry-Perot system weakly coupled to the main resonator. One reflecting element of the Fabry-Perot consists of a diffraction grating to provide selection of the P(20) line. The advantage of this arrangement, shown in Fig 2-4, is that an effective reflection coefficient of 99 percent can be achieved although the reflectivity of the grating is only 92 percent. At the resonance frequencies of the Fabry-Perot, however, the effective reflectivity is much lower, a characteristic which is utilized to suppress the unwanted axial mode adjacent to the active one. The resonator length can be made sufficiently short such that all other modes fall outside the active gain profile. To obtain the required signal coherence, it is envisioned that in the final system the optical carrier is locked to a stable reference laser (LO) while the rf signal is controlled by a precise clock circuit.

FIG. 2-2

UARL WAVEGUIDE CO_2 LASER

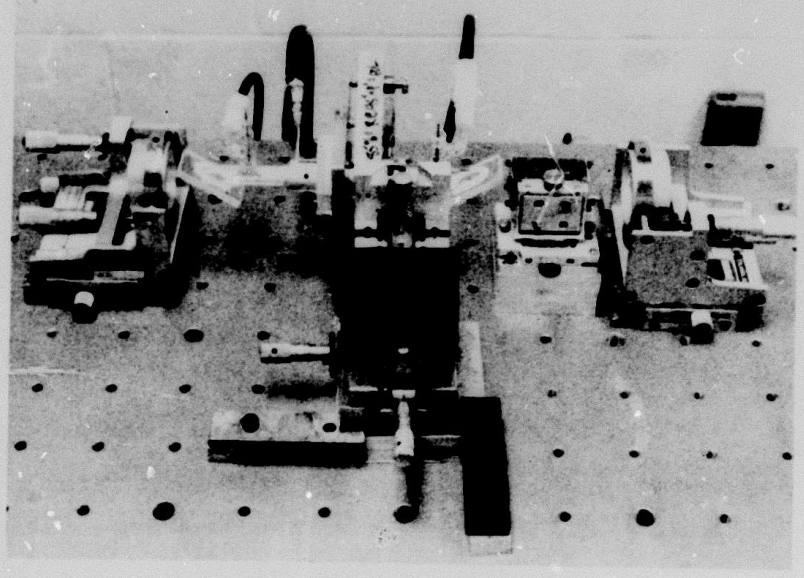

a

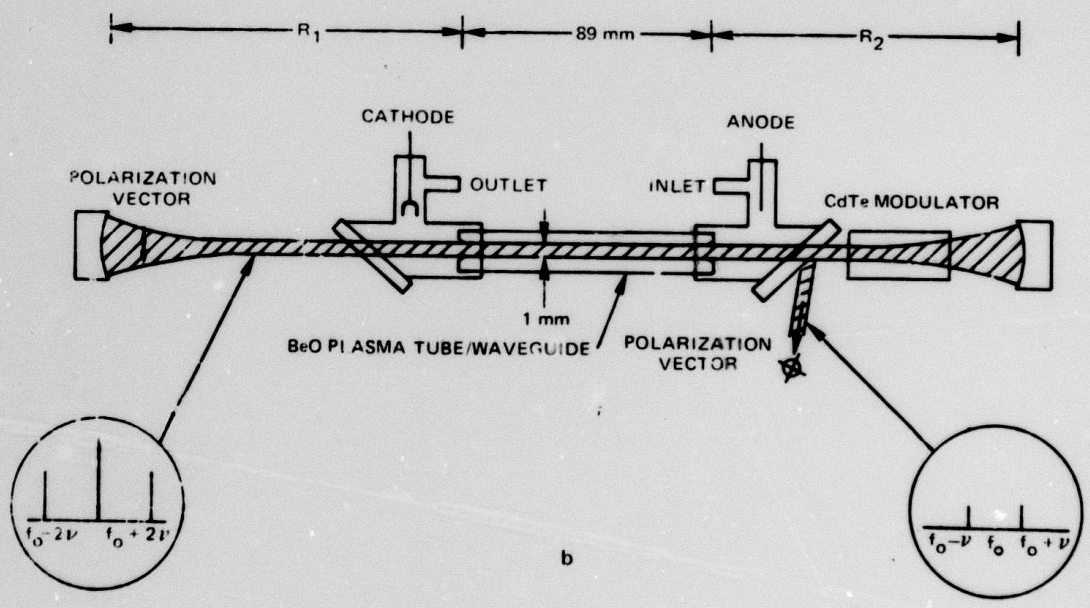

b

M921513–3

FIG. 2–3

OPTICAL SPECTRUM CONTROL

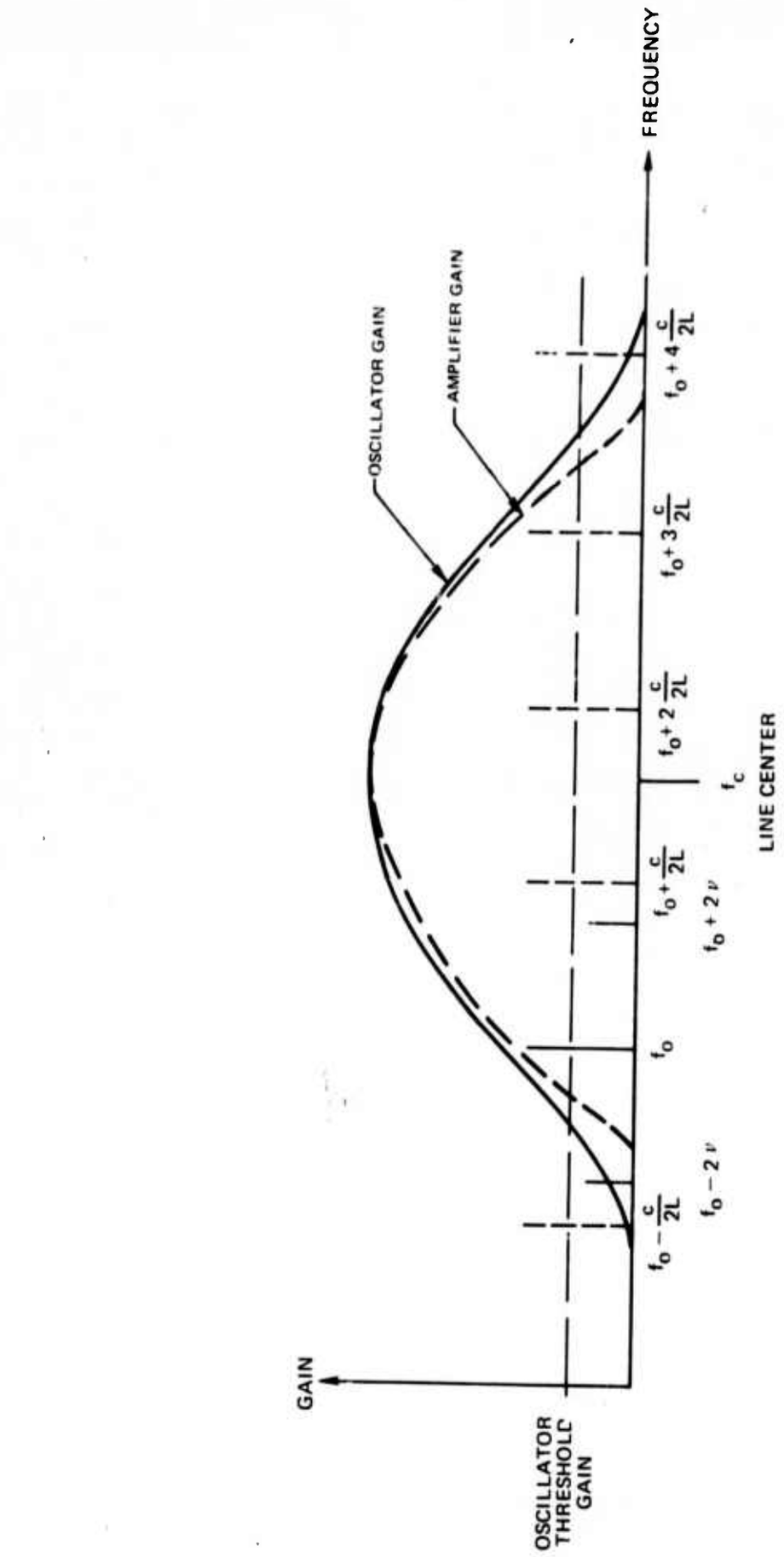

FIG. 2–4

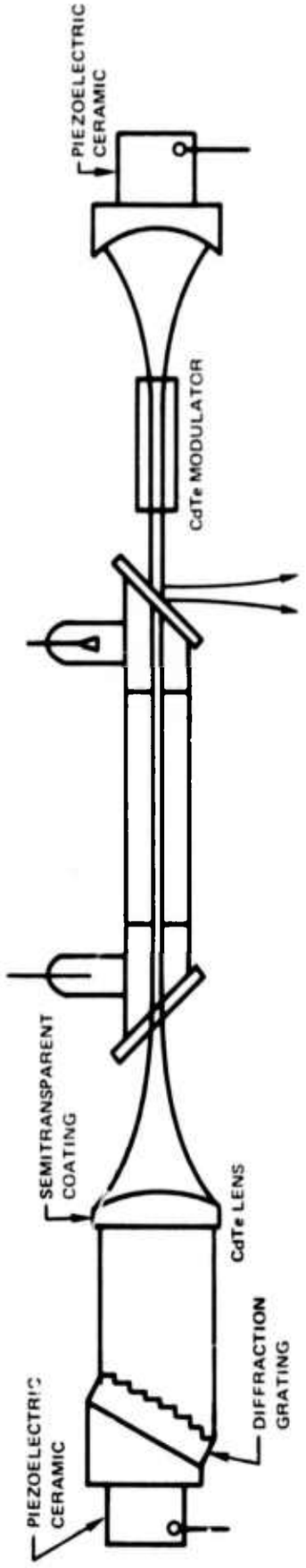

WGL WITH MODE AND LINE SELECTION

SECONDARY FABRY–PEROT

The program described here is principally concerned with two problems: (1) generating a stable optical carrier of the desired frequency displaced from P(20) line center, and (2) obtaining a frequency chirped signal which is precisely correlated to the driving rf.

The typical frequency instability, predominantly due to vibrations of the mechanical resonator structure and thermally induced variations in the effective mirror spacing is minimized by mounting the mirror holders to a rigid baseplate of large thermal mass. The residual "slow" frequency variations are further reduced by resonator length compensation via piezoelectrically actuated mirror displacement. Operation of an optical modulator inside a laser resonator has been demonstrated previously (Ref. 1). The advantage of this scheme is that it requires significantly less drive power to obtain a particular degree of modulation than for the same element employed externally to the resonator.

Several problems, however, have to be overcome in order to take full advantage of internal coupling modulation. There are optical losses, bulk absorption and scattering in the modulator crystal and scattering at interfaces. As a consequence, the stored laser power and the modulated output may be considerably less than one would compute on the basis of lossless elements. For the system shown in Fig. 2-2, it was found experimentally that the internal optical power was reduced by 50 percent upon insertion of the modulator crystal into the resonator.

Heating of the modulator crystal via optical and rf absorption causes a change in the crystal's optical length and hence the resonator frequencies. Care must therefore be taken to obtain as constant a crystal temperature as possible. The residual fluctuations in the resonator length contribute to the long-term carrier instability and can be compensated by piezoelectrical mirror adjustment.

Short-term carrier stability is difficult to control by active means and hence must be built into the laser device. High frequency mechanical vibrations, for instance, are minimized by rigid resonator construction. There is, however, a special contribution to the carrier instability if the electro-optic modulator geometry is not in perfect alignment. In particular, if the applied field is not perfectly normal to any one of the cubic crystal axes, a weak frequency modulation occurs in addition to the desired polarization modulation. The FM appears as a distortion of the radar imaging signal and must be minimized by maintaining proper electro-optic alignment.

A potentially serious drawback to internal modulation is the distortion of the modulated output which results when the modulating frequency approaches the frequency separation between cavity resonances. This effect has been analyzed for cases where the modulating frequency changes slowly such that the resonator establishes a quasi-steady state field at each frequency (Refs. 3 and 4). In our case, however, the frequency change is extremely rapid and steady state cannot be assumed.

Both carrier FMing and modulation distortion are measured by comparison of the modulating rf with the properly demodulated optical signal.

Relying on the passive short-term stability of the resonator, the initial tests have been performed with passively stable systems. It is envisioned that at a later stage the optical carrier is actively controlled by reference to an optical local oscillator via an AFC loop. Such active frequency control requires the minimization of thermal drifts due to heating of the modulator crystal or dimensional changes in the overall mechanical resonator structure. Another source of instability; namely, the occurrence of plasma oscillations is frequently observed in high-pressure waveguide CO_2 lasers but can be eliminated by a proper choice of operating parameters.

Considering the generation and control of the rf modulation, it is noted that demands on performance of the CdTe modulator crystal and rf drive circuit are extraordinary. Although a 300 nsec, 500 MHz frequency sweep is readily achieved for instance by employing varactor tuning of a solid state microwave VCO and subsequent frequency down-shifting, the required linearity and timing presents a formidable task and broad band amplification of the base band signal up to the required level of approximately 1 kW is equally difficult if frequency pulling and other distortion effects are to be minimized in accordance with the required signal quality.

2.2 Coupling Modulation - Theory

For the following discussion it is useful to review the effect of polarization modulation which provides a partial transfer of energy from the linearly polarized oscillating field into an orthogonal polarization component which can then be coupled from the cavity by reflection off an intracavity Brewster plate. The electro-optic crystal (CdTe) is cut such that the light propagates along the $< \bar{1}10 >$ crystal direction, the optical polarization is parallel to $< 001 >$ and the electric field is applied along the $< 110 >$ axis. The optical field vector of the incident light beam then bisects the two principal polarization axes, as shown in the diagram below, yielding the components

$$E_\alpha = \frac{1}{\sqrt{2}} E_o e^{i (kr - \omega_o t + \frac{1}{2}\Gamma)} \quad \text{and} \quad E_\beta = \frac{1}{\sqrt{2}} E_o e^{i (kr - \omega_o t - \frac{1}{2}\Gamma)}, \tag{1}$$

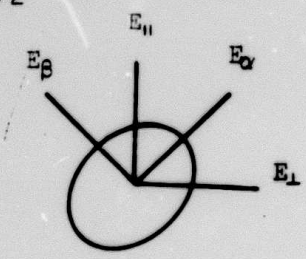

where k is the optical propagation vector, r a coordinate in the propagation direction, $\pm \frac{1}{2} \Gamma$ the principal phase terms, ω_o the carrier frequency and E_o the amplitude of the incident optical field. Upon propagation through the crystal, the beam contains an orthogonal component,

$$\begin{aligned} E_\perp &= 1/\sqrt{2}\ (E_\alpha - E_\beta) \\ &= \tfrac{1}{2} E_o \left[\exp i\ (kr - \omega_o t)\right] \left[e^{i\frac{1}{2}\Gamma} - e^{-i\frac{1}{2}\Gamma}\right] \\ &= i\, E_o \sin \tfrac{1}{2}\Gamma\, e^{i\ (kr - \omega_o t)}, \end{aligned} \tag{2}$$

while the field

$$\begin{aligned} E_\parallel &= 1/\sqrt{2}\ (E_\alpha + E_\beta) \\ &= \tfrac{1}{2} E_o \left[\exp i\ (kr - \omega_o t)\right] \left[e^{i\frac{1}{2}\Gamma} + e^{-i\frac{1}{2}\Gamma}\right] \\ &= E_o \cos \tfrac{1}{2}\Gamma \cdot e^{i\ (kr - \omega_o t)} \end{aligned} \tag{3}$$

remains polarized in the original direction. Suppressing the common spatial phase term, we obtain for the temporal field function

$$\begin{aligned} e_\parallel &= e_o \cos \omega_o t \cdot \cos \tfrac{1}{2}\Gamma \\ e_\perp &= e_o \sin \omega_o t \cdot \sin \tfrac{1}{2}\Gamma. \end{aligned} \tag{4}$$

Evaluating Eq. (4) for the modulation function, $\Gamma = \Gamma_o \cos \omega_m t$, where $\Gamma_o << 1$ corresponds to the applied peak voltage and ω_m is the frequency of the applied rf signal, one gets the approximate expressions

$$\begin{aligned} e_\parallel &= e_o \left(1 - \tfrac{1}{16}\Gamma_o^2\right) \cos \omega_o t - \tfrac{1}{32}\Gamma_o^2 \left[\cos\ (\omega_o t + 2\omega_m) \right. \\ &\qquad \left. + \cos\ (\omega_o - 2\omega_m)\ t\right] \\ e_\perp &= \tfrac{1}{4}\Gamma_o e_o \left[\sin\ (\omega_o + \omega_m)\ t + \sin\ (\omega_o - \omega_m)\ t\right]. \end{aligned} \tag{5}$$

We ascertain from these expressions that the modulation generates symmetric sidebands at the modulation frequency and twice the modulation frequency where the latter is in the same polarization as the carrier and the former in the orthogonal polarization. It has been shown that if a dc bias is applied to the crystal, together with the ac field, $e_\parallel$ contains ω_m and $2\omega_m$ sidebands and $e_\perp$ part of the carrier and ω_m sidebands (Refs. 3, 4). It follows from Eq. (4) that the fraction of the incident power coupled into the orthogonal polarization state, i.e., the depolarization factor is given by

$$D = \sin^2 (\tfrac{1}{2}\Gamma) \tag{6}$$

2.3 Waveguide Laser

A technique for operating a high-pressure CO_2 laser, illustrated in Fig. 2.2, and first demonstrated by P. Smith of Bell Laboratories (Ref. 6), uses a small diameter tube which serves simultaneously as plasma vessel and optical waveguide. In terms of geometrical optics, the guiding effect relates to the high reflection of the capillary wall due to the grazing angle of incidence. The hollow dielectric waveguide described here is unlike the common fiber optic rod where, due to the total internal reflection at the dielectric boundary, genuine lossless waveguide modes are established. The hollow waveguide, on the other hand, suffers a finite reflection loss, i.e., a continual radiation of energy as it propagates through the capillary. Losses, however, are typically as small as 0.02 dB per cm for $\lambda = 10.6$ microns and a capillary diameter of approximately 1 mm (Ref. 7). When two mirrors are placed such that their centers of curvature are located at the left and right capillary opening, respectively, the structure yields a stable resonator configuration which favors oscillation of the lowest order mode although the waveguide is overmoded, i.e., for 10 micron radiation it permits the propagation of very high order modes. The mode selection results from the excellent match of the EH_{11} waveguide and the TEM_{00} free space mode (Ref. 8). Higher order waveguide modes of uniform polarization such as the EH_{12} field do not match as well to the equivalent free space mode (TEM_{01}) and hence suffer a larger coupling loss than the EH_{11} mode. (Selection of polarized modes, of course, relates to the use of a plasma tube with Brewster angle windows or other polarizing elements).

The possibility of operating at high gas pressures results from the scaling properties of the tube confined gas discharge plasma. If the pressure is varied inversely as the tube diameter, the electron energy distribution remains essentially constant and it can be expected that electron collisional excitation processes which are dominant for this laser remain qualitatively unchanged (Ref. 9). Higher pressure yields a broader line width and increased power generation per unit volume.

Prior to commencement of the present contract UARL began the construction of a flowing gas CO_2 waveguide laser using a capillary made of high thermal conductivity BeO to obtain good gas cooling. Optimum current densities in waveguide tubes are approximately 100 times larger than in conventional systems. While the thermal power generated per unit length is approximately equal for waveguide and conventional systems, the heat load is conducted through a much smaller tube surface in the former case. Hence, the temperature drop across the wall surface is large unless a material with good thermal conductivity such as BeO is used as capillary tube. Heat is removed from the outside of the BeO tube by conduction into a water-cooled copper yoke. Glass tubes are cemented to each end of the tube holding the sodium chloride Brewster windows. The electrodes (cylindrical nickel cathode and tungsten pin anode) are placed in side arms which also hold the gas ports.

Although design criteria for waveguide lasers had been established previously (Refs. 6, 7 and 8), a special consideration; namely, the need to optimize the system for uncommonly high operating pressures, requires a careful selection of capillary geometry and operating conditions. BeO capillaries of different sizes and lengths were investigated. Best results were observed for a 1 mm bore 85 mm long tube presently employed in the UARL system. The output power (750 mW) compares with published results (Ref. 7) and is limited by gas cooling techniques, losses due to absorption and scattering in mirror coatings and Brewster plates, the waveguide leakage, and coupling loss involving the transition from waveguide to free space propagation.

2.4 Modulation System

2.4.1 Optical Unit

The choice of CdTe as electro-optic modulator material is based on its relatively low specific half-wave voltage (about half that of GaAs, its closest rival) and an extremely low optical absorption (less than half that of GaAs). In the past, application of this attractive material was limited by the problems of crystal growth, doping techniques, optical fabrication and coatings. Recently, however, some of these problems seem to have been overcome and material of low optical and electrical loss is commercially available. It is too early to state whether the polishing and coating techniques for this extremely brittle material have been significantly improved, but it is interesting to note that two CdTe modulator crystals purchased by UARL for the present program from II-VI Inc., Glenshore, PA, have shown good overall optical quality (better than 95 percent transmission for both AR coated crystals).

2.4.2 rf System

To obtain the rapid and wide frequency sweep together with the required linearity, repeatability and high peak power of the modulating signal is a formidable task. Fortunately, to determine feasibility of the coupling modulation method, the requirements of chirp linearity and repeatability can be relaxed and a simplified rf system, as the one schematically illustrated in Fig. 2-5, suffices.

The VCO output (fast sweep from 502 to 1,000 MHz) is mixed with a 500 MHz local oscillator signal and the resulting difference signal (2 to 500 MHz) is amplified and applied to the modulator crystal. To investigate the modulation response of the master oscillator, a demodulation experiment, as illustrated in Fig. 2-6, is conducted. Here the frequency chirped laser output is heterodyned with an optical oscillator and the IF signal then mixed with a portion of the driving rf signal yielding a low frequency (LF) output,

FIG. 2-5

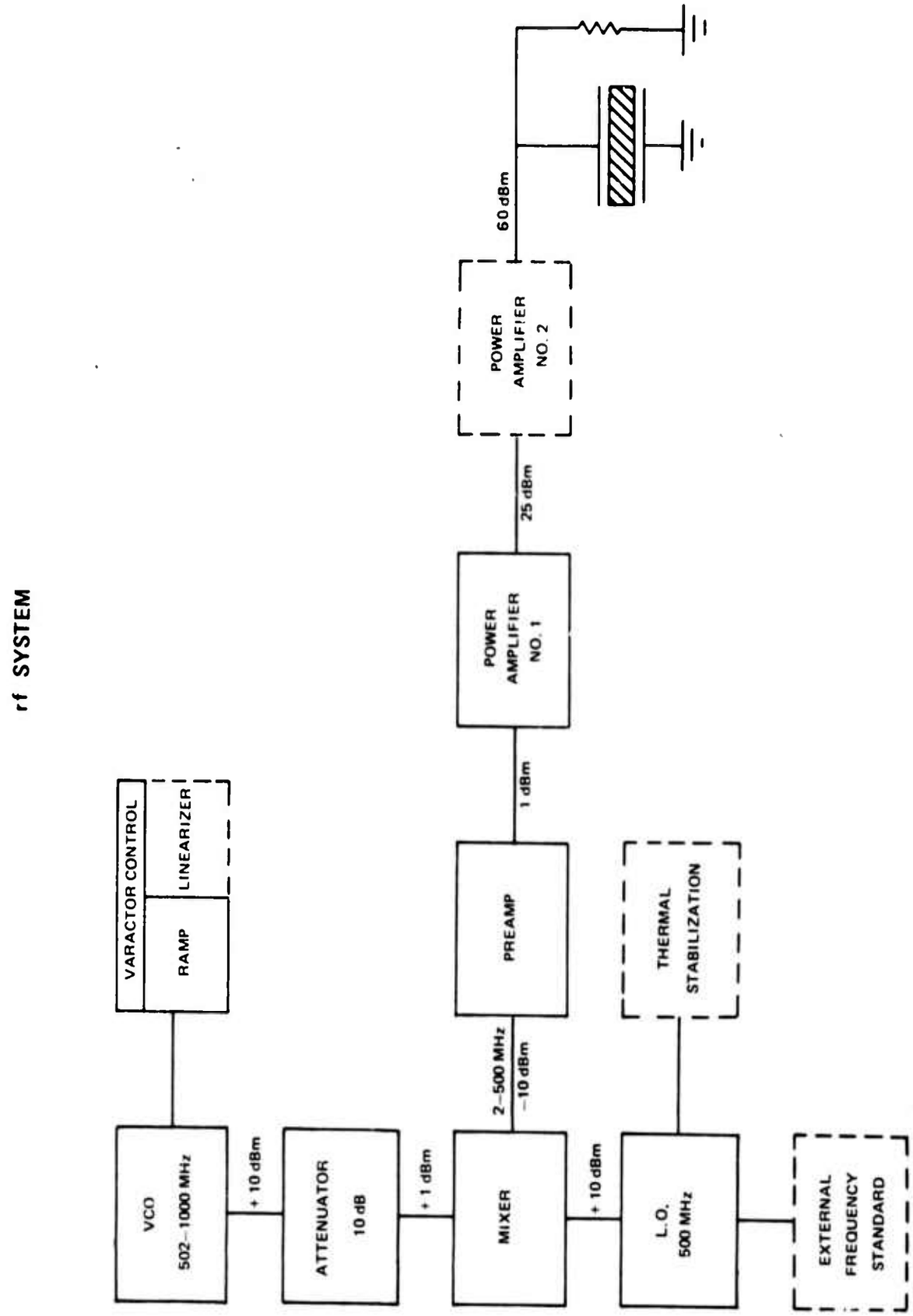
rf SYSTEM
VCO
502-1000 MHz
VARACTOR CONTROL
RAMP
LINEARIZER
+ 10 dBm
ATTENUATOR
10 dB
+ 1 dBm
MIXER
2-500 MHz
-10 dBm
+ 10 dBm
L.O.
500 MHz
THERMAL
STABILIZATION
EXTERNAL
FREQUENCY
STANDARD
PREAMP
1 dBm
POWER
AMPLIFIER
NO. 1
25 dBm
POWER
AMPLIFIER
NO. 2
60 dBm

FIG. 2-6

DEMODULATION SYSTEM

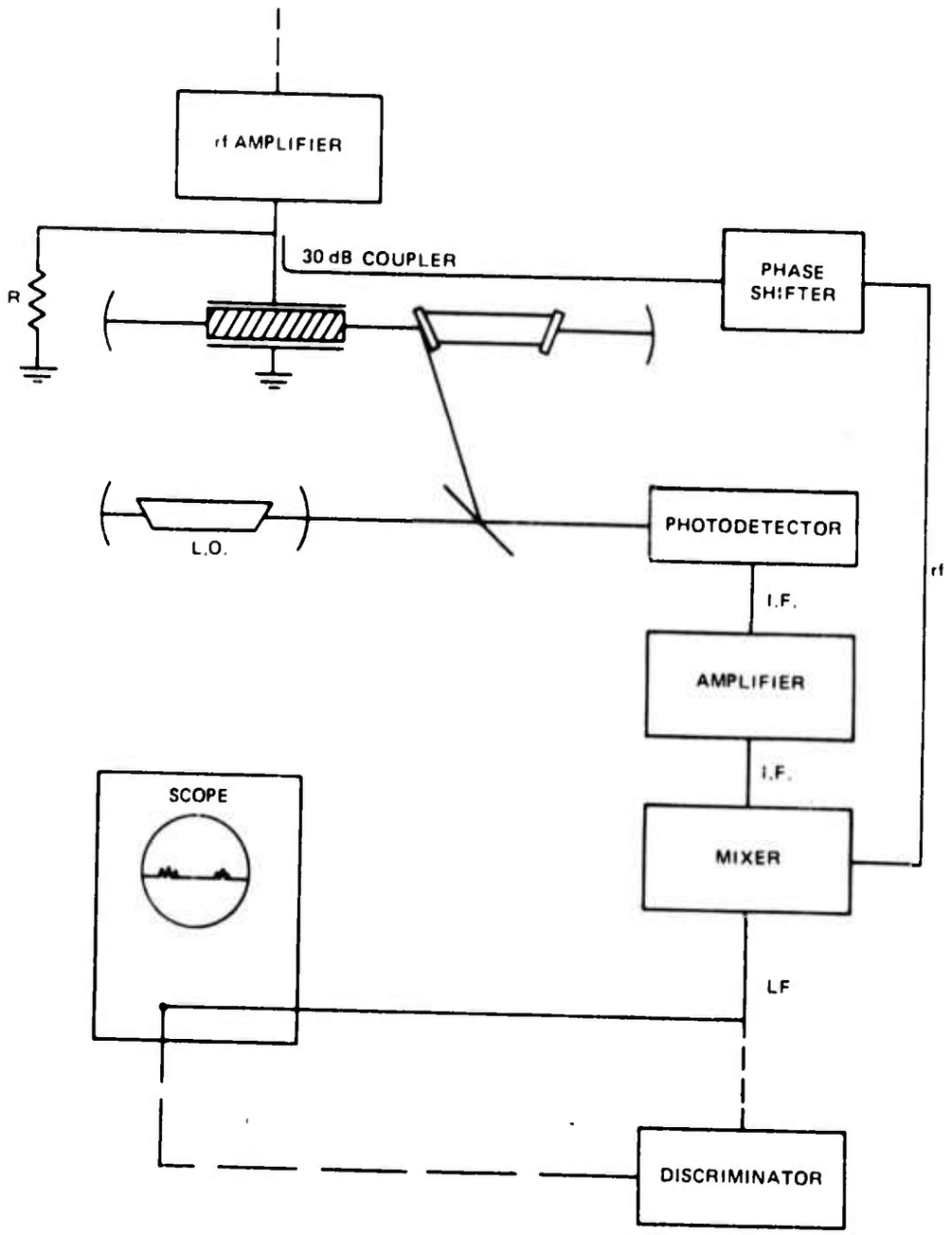

$$V_{LF} \propto \cos[(\omega_o - \omega')t + \varphi_m] + \cos[(\omega_o - \omega')t - \varphi_m]$$

$$\propto \cos(\omega_o - \omega')t \cdot \cos\varphi_m, \qquad (7)$$

where ω_o, ω' and ω_m are the frequencies of carrier, local oscillator and modulation respectively, and φ_m represents the signal distortion, which may be separated into a time varying and constant term, $\varphi_m = \varphi_m'(t) + \varphi_m^o$. Whereas the latter can be readily compensated, the former cannot and in fact represents the parameter to be measured.

2.4.3 rf Power Considerations

Broadband matching of the modulator circuit to the rf drive is accomplished by terminating the last power amplifier into a 50 Ω pad and connecting the CdTe crystal electrodes in parallel. The load impedance then equals

$$Z = \frac{1/R - j\omega C}{1/R^2 + \omega^2 C^2}, \qquad (8)$$

where R = 50 Ω and C = 10 pF. As the frequency is increased, |Z| decreases from its dc value of 50 Ω to 27.5 Ω at 500 MHz.

The above described UARL CO_2 waveguide laser yields 750 mW for an output mirror of 7.6 percent transmission. The power of the traveling wave prior to interception by the output mirror is, therefore, equal to 10 W. It was found that insertion of the modulator crystal reduced this power value to 5 W. Replacement of the transmission mirror by a high reflection element results in an increase, while insertion of a CdTe lens as shown in Fig. 2-4 causes a reduction of the intracavity power. It is reasonable to assume that the additional loss imposed by this element is compensated by the replacement of the transmitting mirror by a highly reflective element. Additional modification of the present system is expected to yield higher output power due to improved alignment accuracy for all cavity elements and better cooling of the active medium. It is, therefore, expected that the final system yields 10 W of intracavity power. Assuming that coupling from the resonator is provided by Fresnel reflection off a CdTe Brewster window surface next to the modulator (57 percent reflection for the "orthogonal" polarization component), it takes a 3.5 percent depolarization to obtain 200 mW output power from that system. From Eq. (6) follows that the depolarization of a linearly polarized beam after a round trip through the CdTe crystal is equal to $D = \pi^2(V_m/V_\pi)^2 \sin^2(\omega_m t)$, where V_m is the peak rf voltage and V_π the half-wave voltage for the CdTe modulator. The time averaged depolarization then is

$$D_{av} = \tfrac{1}{2}\pi^2 \left(\frac{V_m}{V_\pi}\right)^2 . \qquad (9)$$

Inserting the values $D_{av} = 3.5 \times 10^{-2}$ and $V_\pi = 3.9$ kV for the 41-mm long, 3-mm high CdTe crystal we obtain $V_m = 328$ V. If the load resistor is R = 50 Ω, the rf power required during the chirp period is $P_{rf} = \frac{1}{2}(V_m^2/R) = 1{,}070$ W. Since the radar imaging signal consists of 128 pulses of 300 nsec duration each and the imaging rate is 10 per second, the final rf system may be operated at a duty cycle of less than 0.1 percent corresponding to an average rf power of less than 1 W.

Referring again to Fig. 2-5, we note that the rf system employs solid state commercial components except for the final power amplifier which will be developed and fabricated by UARL. Design of this unit is in progress, and assembly and initial testing is expected to be completed by the end of the next reporting period.

2.5 Carrier FMing

Carrier stability is a critical requirement of the above discussed imaging waveform. Short-term frequency fluctuations due to vibrations of the mirrors and the resonator structure can be controlled by employing rigid mirror mounts tightly secured to a massive baseplate. The influence of plasma instabilities is reduced by the use of a sealed-off plasma tube presently under construction.

Let us recall that the modulation discussed here exploits a particular characteristic of the selected electro-optic geometry; namely, the fact that the phase changes for the two principal polarizations are equal and opposite. If the applied electric field is <u>not</u> precisely normal to any one of the cubic axes of the CdTe crystal, one may express the positive and negative phase terms as (Ref. 10) $\frac{1}{2}\Gamma + \Delta$ and $\frac{1}{2}\Gamma - \Delta$, rendering Eqs. (2) and (3) in the form

$$E_{\parallel} = E_o\, e^{i(kr-\omega_o t)}\, e^{i\Delta} \cos \tfrac{1}{2}\Gamma$$

$$E_{\perp} = E_o\, e^{i(kr-\omega_o t)}\, e^{i\Delta} \sin \tfrac{1}{2}\Gamma. \qquad (10)$$

Since the parameter Δ varies sinusoidally with the applied voltage---as does the parameter Γ---a weak frequency modulation results, in addition to the desired polarization modulation. The FM appears as a distortion of the radar imaging signal and can be measured by demodulation of the IF signal in a discriminator as indicated schematically in Fig. 2-6.

2.6 Modulation Distortion

In the above discussion, we have treated the intracavity polarization modulation as an effect related to a single transmission through the modulator. (Two way transmission is equivalent to propagation through a crystal of twice the actual length provided a reflector is placed close to the modulator). However, a special situation

arises when the modulation frequency or its first subharmonic is equal to the frequency difference of adjacent axial resonances, c/2L, where c is the velocity of light and L the optical resonator length. In that case, a cumulative effect occurs involving many transits through the modulator resulting in increased amplitude modulation of the parallel field component, increased intensity of the output wave, and a change in the relative phase of the rf and optical signals. (No mode locking occurs if all but one axial mode are passive). These effects have been analyzed for quasi-steady state cases where the rate at which the modulating frequency changes is sufficiently small (Refs. 3 and 4). In our case, however, the frequency change is extremely rapid and steady state cannot be assumed. Here, as in the case of FM distortion, we seek an answer from the demodulation experiment suggested in Section 2.4.2.

3.0 EXPERIMENTAL RESULTS

3.1 Introduction

During the reporting period work was concentrated on assembly and testing of a suitable waveguide laser. The system was then provided with a low loss cadmium telluride electro-optical modulator, and coupling modulation was observed for two discrete rf frequencies.

It is generally recognized that optical and/or rf heating of the intracavity modulator element and the ensuing change in optical resonator length poses a potential problem in attaining the required carrier stability. Since the rf signal consists of a pulse burst, we are concerned with rapid temperature variations beyond the response of a piezoelectric control loop which may readily compensate slow thermal drifts.

It should be noted here that these thermal effects are much weaker for CdTe than for GaAs frequently employed in previous modulated CO_2 lasers, since:

(1) the absorption coefficient for CdTe is one half that of GaAs,

(2) only one quarter of the electrical power is required to obtain the same modulation depth as for a GaAs crystal of equal dimensions, and

(3) the temperature variation of the refractive index and the thermal expansion coefficients are smaller for CdTe than for GaAs.

With the rf signal off, we found that, after an initial warm-up period of some 15 minutes, the thermal drift was very slow; it took several minutes for a change of a few microns in the optical resonator length. The observed passive stability, then, seems adequate for the modulation response measurement described in Section 2, since observation times of less than 5 msec are required.

To obtain such passive thermal stability the crystal was clamped to a structure of sufficiently large thermal mass and this assembly placed in a thermally isolating enclosure to decouple it from the temperature fluctuations of the surrounding air.

3.2 Laser Parameters

During the next reporting period a line and mode selected CO_2 waveguide laser will be assembled to obtain the carrier displacement required for the wide band coupling modulation described in Section 2.

A preliminary design for such a unit is illustrated in Fig. 2-4 showing a diffraction grating for line selection and a secondary Fabry-Perot coupled to the main optical resonator for mode selection and mode control.

In order to decide whether the above system may be implemented by modifying the present UARL CO_2 waveguide laser, it was necessary to obtain accurate values for gain, loss and saturation parameter of the present system.

The gain factor was measured directly with the help of a low-power probe laser while loss and saturation parameters were then determined by introducing an additional, known resonator loss and matching the measured change in the output power, P_o, to the relation (Ref. 11)

$$P_o = T \times S \times \pi \times \omega_o^2 \left[\frac{G}{L + \eta} - 1 \right] , \qquad (11)$$

where T is the output mirror transmission; L and G the round-trip loss and gain factors, respectively, expressed in dB; η the transmission also expressed in dB; ω_o the beam radius inside the waveguide capillary; and S the saturation parameter. The additional loss was introduced by applying a dc voltage to the CdTe modulator thus generating a well defined depolarization loss.

We investigated the system at the following operating conditions:

Average Gas Pressure:	40 torr
Gas Mixture:	1:1:3; CO_2,N_2,He
Volumetric Flow Rate:	10 cm^3/sec
Discharge Current:	2.8 mA for the 1 x 83 mm capillary cooled at 20°C
Output Transmission:	T = 0.076.

It was found that the round-trip gain is 2.3 dB, i.e., 13.8 dB/m, the total loss 1.22 dB, and the saturation power 2.83 W which yields a saturation density of S = 1.5 kW/cm^2 for a beam radius of approximately 0.25 mm.

The loss consists of the following contributions:

CdTe Crystal:	0.40 dB
Laser Mirrors:	0.20 dB total (estimated)
Coupling Loss-Guided to Free Propagation:	0.15 dB total
Waveguide Leakage:	0.30 dB

This leaves an apparently unidentified component of 0.17 dB. Upon close inspection of the Brewster windows, it was found, however, that the window surface next to the cathode had a slightly diffuse appearance presumably due to the influence of cathode sputtering. When the window was replaced with a new one, the laser power increased indicating that the residual loss component related indeed to the poor window quality.

3.3 Coupling Modulation Experiments

While the high-power wide band rf amplifier required for the frequency chirped modulation is under development, a preliminary test of the system was performed by employing a resonant excitation of the CdTe crystal at two discrete frequencies, 48 and 120 MHz. In both cases, the crystal representing a capacitor with a high resistance shunt, was resonated with an air coil, and the residual resistive load matched to a 50 line by tapping into the coil which then acted as an auto-transformer providing the appropriate impedance step-up.

In this way a rms voltage of 300 V was developed across the crystal for an input power of only 3 W, due to the high Q-value (> 100) of the resonant circuit.

The depolarized field was coupled from the laser by Fresnel reflection off the NaCl Brewster window adjacent to the modulator and detected with a Ge:Hg(Sb) element cooled to liquid helium temperature.

Figures 3-1 and 3-2 display the detector signal for both the 48 and 120 MHz modulation. Note that the demodulated signal is of the same frequency as the modulating one, which corresponds to the case of rf modulation with dc bias as shown in Refs. 3 and 4. Although no external dc bias was applied in this experiment, an effective bias was provided by the crystal's stress birefringence. The second harmonic of the rf signal is not noticable since the detection system was limited to the fundmental component in both cases.

FIG. 3 - 1

48 MHz COUPLING MODULATION

1 W rf POWER INTO RESONANT CIRCUIT, WITHOUT PREAMP

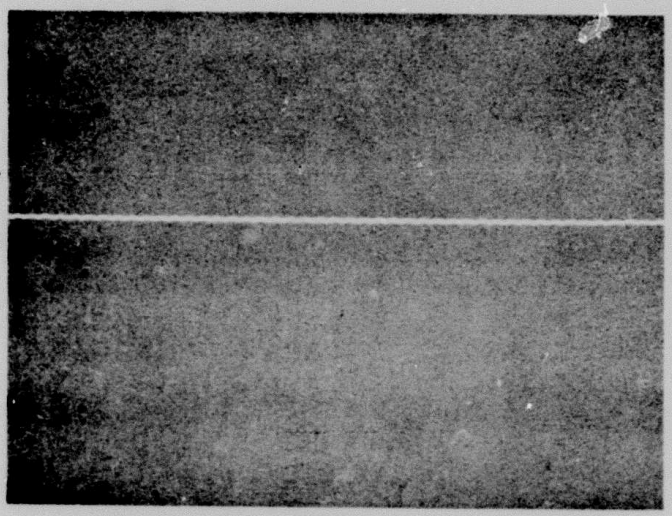

a) OPTICAL SIGNAL BLOCKED
(RIPPLE CAUSED BY rf PICK-UP)

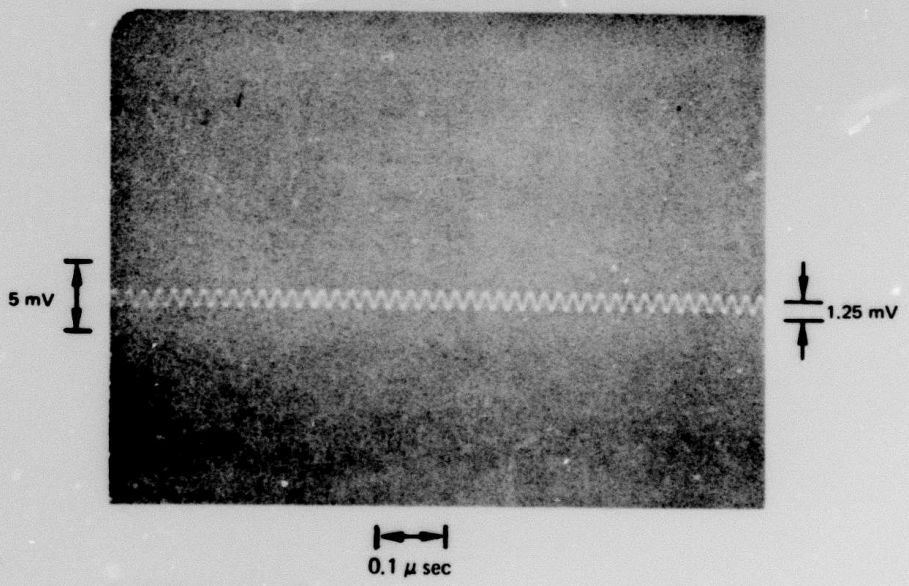

b) OPTICAL SIGNAL ON

FIG. 3–2

120 MHz COUPLING MODULATION

1/2 W rf POWER INTO RESONANT CIRCUIT; WITH PREAMP (15 dB VOLTAGE GAIN)

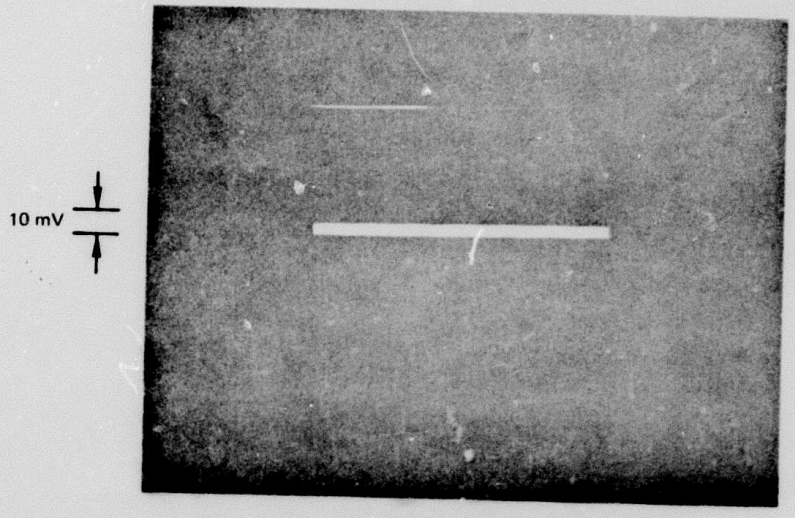

a) OPTICAL SIGNAL BLOCKED
(FINITE LINE THICKNESS CAUSED BY rf PICK–UP)

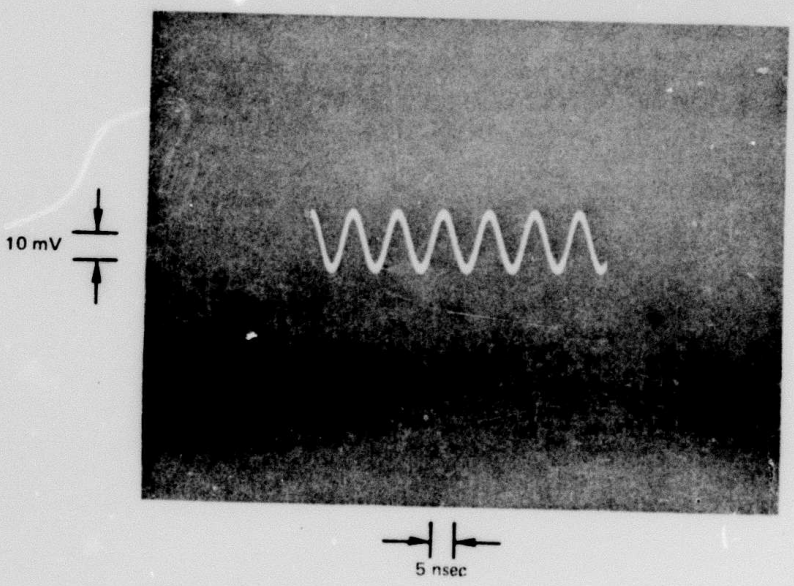

b) OPTICAL SIGNAL ON

4.0 DISCUSSION AND FUTURE PLANS

During this reporting period a CO_2 waveguide laser was operated with an intracavity electro-optic polarization modulator. Coupling modulation at 48 and 120 MHz was observed. This represents a significant step towards the contract goal to obtain a linear ramp frequency modulation (500 MHz in 300 nsec) for a stable CO_2 oscillator. The preliminary measurements have yielded detailed information on laser gain, loss and saturation power; the efficiency of the CdTe modulator; and the frequency and amplitude stability of the system on which we based the design of the stable frequency swept CO_2 system now under construction. In fact, it appears that the required mode control can be achieved by a modification of the present laser, replacing the output mirror with a Fabry-Perot system which is weakly coupled to the main resonator and which contains, as one of its reflecting elements, a diffraction grating for selection of the P(20) line.

A rf drive system with the required frequency sweep of 500 MHz in 300 nsec has been assembled except for the final power amplifier which will be fabricated in-house during the next reporting period and is expected to yield a peak power of 1 kW.

Upon completion of the line and mode stabilization of the waveguide laser and of the high-power modulator drive during the next reporting period, the system will be used as a test bed for the investigation of the frequency swept broadband coupling modulation. Specifically, carrier stability and the response of the modulation near frequencies equal to the axial mode spacing will be measured by comparison of the properly demodulated optical with the rf drive signal.

REFERENCES

1. Gürs, K., Z. Physik 172, 145 (1963).

2. Wiedes, I. and G. B. McCurdy, Phys. Rev. Lett. 16, 565 (1966).

3. Kaminow, I. P., Appl. Optics 4, 123 (1965).

4. Nash, F. R. and P. W. Smith, IEEE J. of Quantum Electronics, QE-4, 26 (1967).

5. Smith, P. W. IEEE J. of Quantum Electronics, QE-1, 343 (1965).

6. Smith, P. W., Appl. Phys. Letters 19, 132 (1971).

7. Burkhardt, E. G., T. D. Bridges and P. W. Smith, Optics Communications 6, 193 (1972).

8. Abrams, R. C. and A. N. Chester, Opt. Soc. of Amer. Spring Meeting, Denver, Colorado, 13-16 March 1973.

9. Cobine, J. D., "Gaseous Conductors", Dover, New York, 1958.

10. Kaminow, I. P. and E. H. Turner, Proc. of the IEEE 54, 1374 (1966).

11. N. W. Rigrod, J. Appl. Physics 36, 2497 (1965).